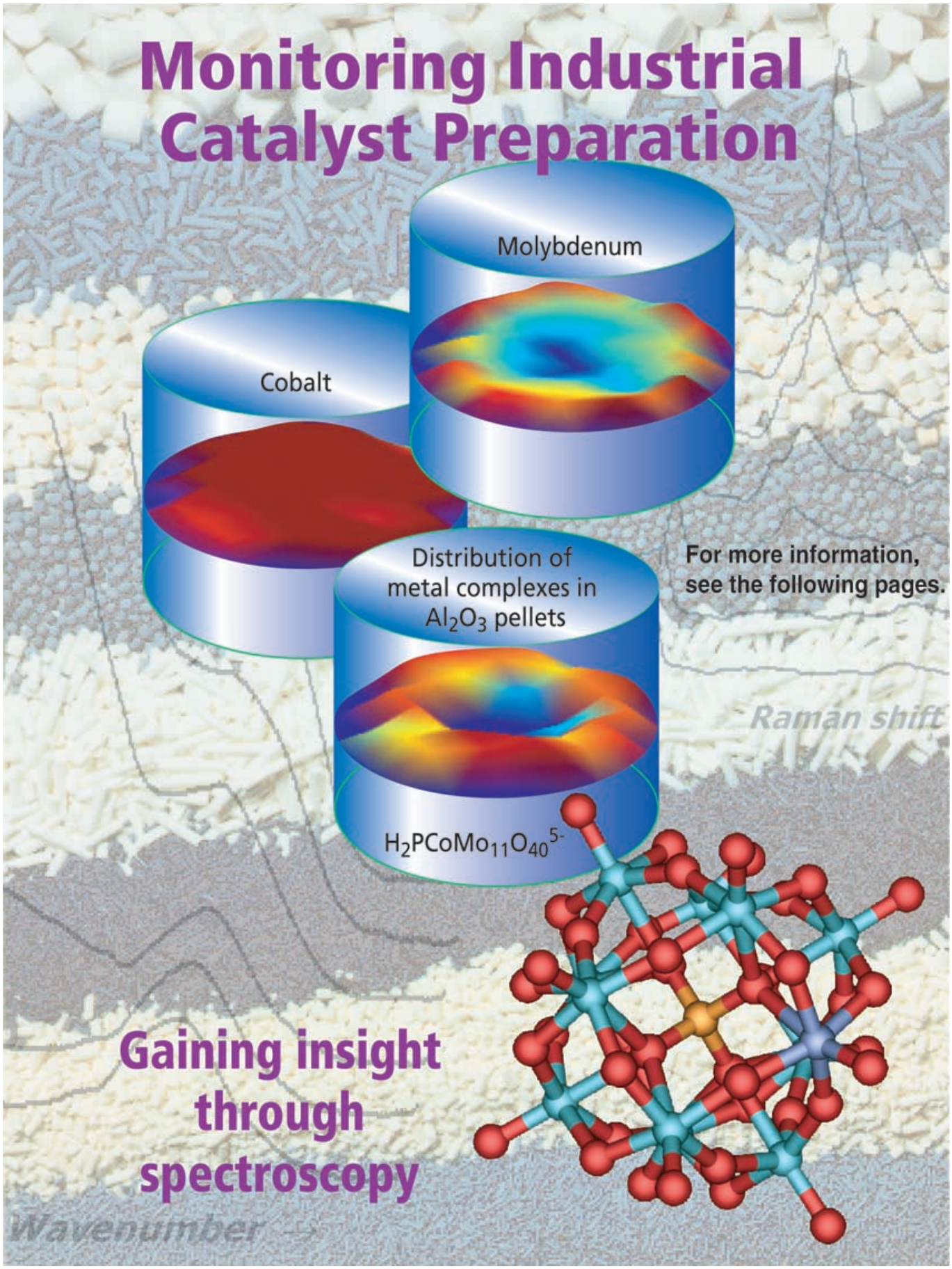


 **DOI: 10.1002/chem.200500116**  

CHEMISTRY
A EUROPEAN JOURNAL

# Spatially Resolved Raman and UV-visible-NIR Spectroscopy on the Preparation of Supported Catalyst Bodies: Controlling the Formation of $H_2PMo_{11}CoO_{40}^{5-}$ Inside $Al_2O_3$ Pellets During Impregnation

**Jaap A. Bergwerff,[a] Leon G. A. van de Water,[a] Tom Visser,[a] Peter de Peinder,[a] Bob R. G. Leliveld,[b] Krijn P. de Jong,[a] and Bert M. Weckhuysen*[a]**

**Abstract:** The physicochemical processes that occur during the preparation of CoMo–$Al_2O_3$ hydrodesulfurization catalyst bodies have been investigated. To this end, the distribution of Mo and Co complexes, after impregnation of γ-$Al_2O_3$ pellets with different CoMoP solutions (i.e., solutions containing Co, Mo, and phosphate), was monitored by Raman and UV-visible-NIR microspectroscopy. From the speciation of the different complexes over the catalyst bodies, insight was obtained into the interaction of the different components in the impregnation solution with the $Al_2O_3$ surface. It is shown that, after impregnation with a solution containing $H_2PMo_{11}CoO_{40}^{5-}$, the reaction of phosphate with the $Al_2O_3$ leads to the disintegration of this complex. The consecutive independent transport of $Co^{2+}$ complexes (fast) and $Mo^{6+}$ complexes (slow) through the pores of the $Al_2O_3$ is envisaged. By the addition of extra phosphate and citrate to the impregnation solution, the formation of the desired heteropolyanion can be achieved inside the pellets. Ultimately, the $H_2PMo_{11}CoO_{40}^{5-}$ distribution could be controlled by varying the aging time applied after impregnation. The power of a combination of spatially resolved spectroscopic techniques to monitor the preparation of supported catalyst bodies is illustrated.

**Keywords:** heterometallic complexes · hydrodesulfurization · Raman microscopy · supported catalysts · UV/Vis spectroscopy

## Introduction

Heterogeneous catalysts are of paramount importance for our present day society, as they are being used in crucial industrial processes, such as oil refining, chemical manufacture, and environmental applications.[1–3] Among these solid catalysts, supported catalysts form an important subclass. The structure of these systems is highly complex with, for instance, nanometer-scale metal clusters deposited into the 10–100 nm pores of millimeter-scale support bodies. For optimum activity of the final catalyst, control on all these different length scales is required.[4–7] It is therefore surprising that in industrial catalyst preparation at first sight straightforward techniques are being used. Pore-volume impregnation, in which the active phase is applied to pre-shaped porous support bodies by addition of a metal-salt solution, is generally the method of choice.[1–3] Typically, in catalyst preparation studies, parameters in the preparation cycle, such as the composition of the impregnation solution and the drying conditions, are varied, after which the effect of these alterations on the final state of the catalyst and the efficiency of the catalyst is monitored. However, in many cases, a thorough understanding of the physicochemical processes that occur during the preparation of supported catalysts is lacking. It is of great importance to obtain these insights, as one clearly strives towards a more controlled way of catalyst preparation.[4–7] In this context, several studies have been dedicated to the physicochemical processes during the preparation of supported catalyst bodies.[8–12] However, in all these cases, characterization was carried out after the preparation procedure. Recently, in our group, microspectroscopic techniques were developed that allow one

[a] J. A. Bergwerff, Dr. L. G. A. van de Water, Dr. T. Visser, P. de Peinder, Prof. Dr. K. P. de Jong, Prof. Dr. B. M. Weckhuysen
Department of Inorganic Chemistry and Catalysis
Debye Institute, Utrecht University
Sorbonnelaan 16, 3508 TB Utrecht (The Netherlands)
Fax: (+31) 302-511-027
E-mail: b.m.weckhuysen@chem.uu.nl

[b] Dr. B. R. G. Leliveld
Albemarle Catalysts BV, Nieuwendammerkade 1–3
1022 AB Amsterdam (The Netherlands)

Supporting information for this article is available on the WWW under http://www.chemeurj.org/ or from the author.



DOI: 10.1002/chem.200500116

to monitor the nature and distribution of metal precursors inside supported catalyst bodies during their preparation.[13,14] The method used for studying the equilibration process after impregnation of support bodies with Raman microscopy and spatially resolved UV-visible-NIR spectroscopy, is depicted in Figure 1.

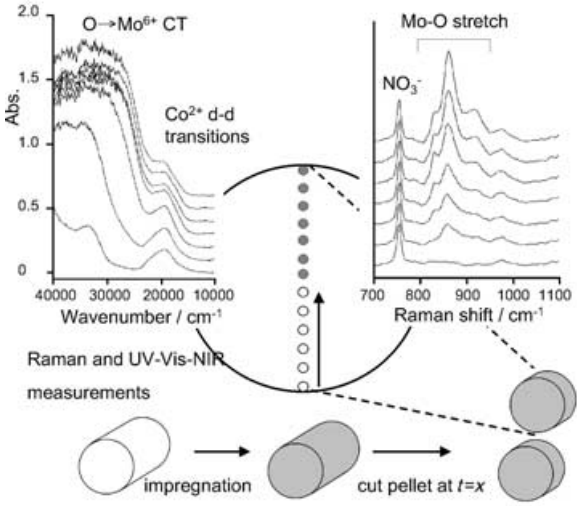


Figure 1. Layout of spatially resolved Raman and UV-visible-NIR measurements on catalyst bodies.

In hydrotreating, (Co)$MoS_2$/$Al_2O_3$ catalysts are often used that are applied in the form of millimeter-size catalyst bodies. They are generally prepared by impregnation of γ-$Al_2O_3$ extrudates with a solution containing Mo and Co complexes, followed by aging, drying, and sulfidation. In these catalysts, Co atoms are located at the edges of the $MoS_2$ slabs and are thought to constitute the active sites in these promoted catalysts.[15–17] To enable this promoting function of Co, it is of crucial importance that Co and Mo are in close contact after sulfidation. Therefore, a homogeneous distribution of Mo and Co over the catalyst bodies is a prerequisite for maximal activity. Furthermore, the nature of the Mo and Co complexes after drying strongly influences the activity of the final catalyst. It is known, for instance, that the formation of crystalline Co phases, such as $CoAl_2O_3$ and $CoMoO_4$, prevents the promoting effect of Co in the final catalyst. The addition of complexing agents, on the other hand, is reported to retard the sulfidation of Co, leading to a more active CoMoS phase in the final catalyst.[18–20] In this context, the use of heteropolyanions containing both Mo and Co, such as $H_2PMo_{11}CoO_{40}^{5-}$ or $Co(OH)_6Mo_6O_{18}^{3-}$ as precursors for hydrodesulfurization catalysts, has been studied in recent years.[21–23] Increased activity was indeed reported for the catalysts prepared using this approach. However, the stability of these compounds during the preparation was found to be a problem, especially for the former complex. Phosphate-containing Keggin-type complexes are reported to decompose upon adsorption onto the $Al_2O_3$ surface.[22,24] The characteristic Raman and UV-visible-NIR spectra of this complex in solution make it a suitable candidate to illustrate the power of combined spectroscopic techniques in catalyst preparation studies. In CoMo/$Al_2O_3$ catalyst bodies, Raman microscopy and spatially resolved UV-visible-NIR spectroscopy can be combined to monitor both the distribution and the nature of Mo complexes, through their characteristic Mo–O stretch vibrations, and Co complexes, by the position of the $Co^{2+}$ d–d transitions. Both techniques are thus valuable tools in studying the preparation of CoMo/$Al_2O_3$ catalyst bodies (Figure 1). In this study, we illustrate how the disintegration and formation of a Keggin-type $H_2PMo_{11}CoO_{40}^{5-}$ heteropolyanion inside the pores of $Al_2O_3$ pellets can be monitored by using the aforementioned techniques. Subsequently, the insights that were obtained in this way were used to control the distribution of this complex after impregnation.

## Results and Discussion

**Raman and UV-visible-NIR on CoMoP solutions**: To evaluate the influence of the phosphate concentration on the formation of $H_2PMo_{11}CoO_{40}^{5-}$, calculations were carried out to determine the constitution of a CoMoP solution as a function of the phosphate concentration by using values for the formation and stability constants of the different complexes taken from literature.[25–27] In Figure 2, the concentration of

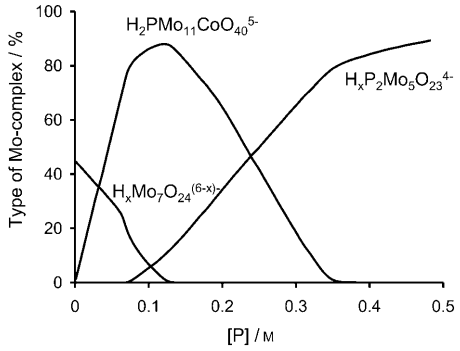


Figure 2. Composition of a 1.0 M Mo, 0.5 M Co solution as a function of increasing phosphate concentration as calculated from literature data.

the predominant Mo complexes in a 1.0 M Mo/0.5 M Co solution is presented when the phosphate concentration is varied between 0 and 0.5 M. These calculations indicate the presence of isopolyanions in the acidic CoMo solution before addition of any phosphate. At low phosphate concentrations, practically all phosphate that is added to the solution is used in the formation of the Keggin-type complex, as the equilibrium in Equation (1) shifts to the right. A maximum in the $H_2PMo_{11}CoO_{40}^{5-}$ concentration is reached at a phosphate concentration of 0.12 M, when close to 90% of all Mo present in solution is contained in this complex. When the phosphate concentration is increased above this value, disintegration of $H_2PMo_{11}CoO_{40}^{5-}$ is expected, due to the

  

formation of $H_2P_2Mo_5O_{23}^{4-}$, as the equilibrium in Equation (2) is shifted to the right.

$$11\,H_xMo_7O_{24}^{(6-x)-} + 7\,H_yPO_4^{(3-y)-} + 7\,[Co(H_2O)_6]^{2+} \rightleftharpoons 7\,H_2PMo_{11}CoO_{40}^{5-} + 54\,H_2O \quad (1)$$

$$5\,H_2PMo_{11}CoO_{40}^{5-} + 17\,H_xPO_4^{(3-x)-} + 15\,H_2O \rightleftharpoons 11\,H_yP_2Mo_5O_{23}^{(6-y)-} + 5\,[Co(H_2O)_6]^{2+} \quad (2)$$

Calculations on the speciation of MoP solutions indicate that $H_xP_2Mo_5O_{23}^{(6-x)-}$ is the thermodynamically favored species for all Mo/P ratios. However, the presence of $Co^{2+}$ allows for the formation of $H_2PMo_{11}CoO_{40}^{5-}$, which appears to be a highly stable complex, although the formation of this heteropolyanion in CoMoP solutions will only take place at specific Mo/P concentration ratios.

Raman and UV-visible-NIR spectroscopy measurements were carried out on CoMoP reference solutions to obtain reference spectra of the different complexes and evaluate the power of both techniques in analyzing these systems. The Raman and UV-visible-NIR spectra of these solutions are presented in Figure 3. Raman spectra are presented in

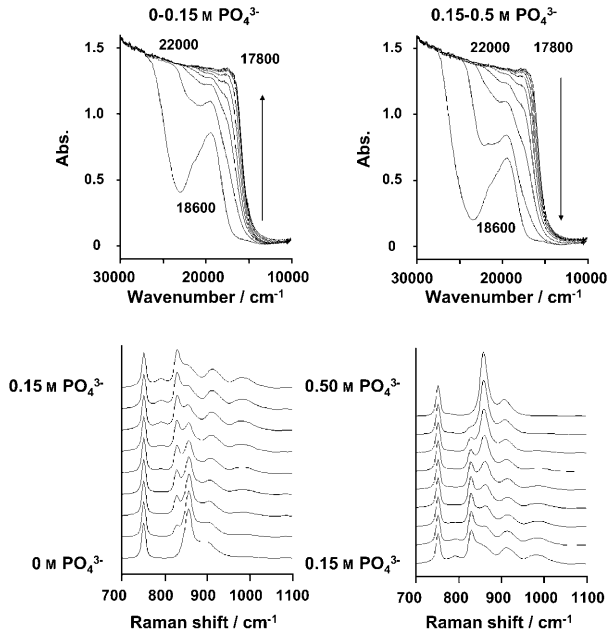


Figure 3. UV-visible-NIR and Raman spectra of 1.0 M Mo, 0.5 M Co reference solutions in which the phosphate concentration is varied between 0 and 0.50 M.

the 700–1100 $cm^{-1}$ range, in which Mo–O stretch vibrations are typically observed. Information that is contained in other parts of the spectra will be discussed in the text only. The Raman spectrum of the solution without phosphate shows peaks at 943, 900, and 356 $cm^{-1}$, which indicate that $H_xMo_7O_{24}^{(6-x)-}$ is the predominant complex in this solution.[28] However, different isopolyanions are probably present, as the feature that is observed between 800 and 1000 $cm^{-1}$ is rather broad. In the UV-visible-NIR spectra, a band with its maximum at 18600 $cm^{-1}$ is observed; the typical position for the $^4T_{1g} \rightarrow {}^4T_{1g}$ (P) d–d transition of octahedrally coordinated $Co^{2+}$ in $[Co(H_2O)6]^{2+}$.[29] Besides this band, an $O \rightarrow Mo^{6+}$ charge-transfer band is observed in the UV region, with its onset at 23000 $cm^{-1}$.

In the Raman spectra of the solutions with a phosphate concentration between 0 and 0.15 M phosphate, peaks at 971 (with a shoulder at 954), 886, and 228 $cm^{-1}$ appear, which become more intense as the phosphate concentration increases. Simultaneously, two bands at 17800 and 22000 $cm^{-1}$ appear in the UV-visible-NIR spectra, and the onset of the $O \rightarrow Mo^{6+}$ charge-transfer band shifts into the visible region. These features confirm the formation of the heteropolyanion, indicated by the calculations.[21,27] The coordination of $Co^{2+}$ in this complex is probably pseudo-octahedral, as the orientation of $Co^{2+}$ towards five of the coordinating oxygen atoms is fixed by the structure of the Keggin ion. However, the distance of the water molecule completing the sixfold coordination towards the outside of the complex is variable. This distortion from perfect octahedral coordination may be an explanation for the relatively high extinction coefficient observed for the band at 17800 $cm^{-1}$. The formation of large Mo–O clusters results in the observed red-shift in the onset of the $O \rightarrow Mo^{6+}$ charge-transfer band.[30]

A maximum in the intensity of the 17800 $cm^{-1}$ band in the UV-visible-NIR spectra and the 971 $cm^{-1}$ band in the Raman spectra is observed when a phosphate concentration of approximately 0.15 M is reached. A decrease of the $H_2PMo_{11}CoO_{40}^{5-}$ features in the Raman and UV-visible-NIR spectra is observed at higher phosphate concentrations. At a phosphate concentration of 0.5 M, the UV-visible-NIR spectra shows that all the Co is contained in $[Co(H_2O)_6]^{2+}$ and the disintegration of the heteropolyanion is complete. The corresponding Raman spectrum shows peaks at 942, 893, 395, and 370 $cm^{-1}$, which are characteristic for $H_xP_2Mo_5O_{23}^{(6-x)-}$ at low pH.[13]

It is shown that the formation and disintegration of $H_2PMo_{11}CoO_{40}^{5-}$ in solution can be monitored by both Raman and UV-visible-NIR spectroscopy. The intensity of the band at 17800 $cm^{-1}$ in the UV-visible-NIR spectra of the reference solutions is a measure for the $H_2PMo_{11}CoO_{40}^{5-}$ concentration. Due to the overlap of this band with the $[Co(H_2O)_6]^{2+}$ band at 18600 $cm^{-1}$ and the relatively high extinction coefficient of this transition, determination of the intensity of the transition was carried out at 16000 $cm^{-1}$, at the down slope of the peak. In Figure 4, the absorption at this position in the spectrum is presented for the CoMoP reference solutions with different phosphate concentrations. Unfortunately, as the extinction coefficient for this complex is not known, it was not possible to determine the $H_2PMo_{11}CoO_{40}^{5-}$ concentration in these solutions quantitatively.

The presence of $NO_3^-$ as an internal standard allows for the quantitative analysis of the Raman spectra. Analysis was carried out in the range of 750–1150 $cm^{-1}$ on spectra after

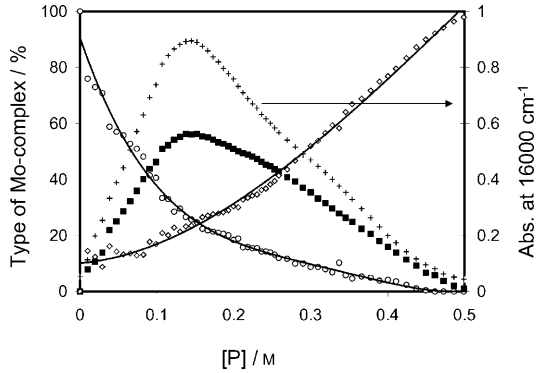


Figure 4. Speciation of Mo complexes (○ $H_xMo_7O_{24}^{(6-x)-}$, ■ $H_2PMo_{11}CoO_{40}^{5-}$, ◇ $H_xP_2Mo_5O_{23}^{(6-x)-}$) in CoMoP reference solutions as a function of the phosphate concentration, as derived from quantitative analysis of Raman spectra. The values for the absorption at 16000 $cm^{-1}$ in the corresponding UV-visible-NIR spectra (+) are included for comparison.

background correction and scaling to the $NO_3^-$ peak at 1048 $cm^{-1}$. From the calculations based on literature data, it was already clear that $H_xMo_7O_{24}^{(6-x)-}$, $H_2PMo_{11}CoO_{40}^{5-}$, and $H_xP_2Mo_5O_{23}^{(6-x)-}$ in their different protonation states are the main complexes present in the CoMoP reference solutions. However, the similarity in the Raman spectra of these complexes makes it difficult to obtain understandable results from a principal component analysis of these spectra without any additional input. For this reason, pure component spectra of $H_xMo_7O_{24}^{(6-x)-}$, $P_2Mo_5O_{23}^{6-}$, $HP_2Mo_5O_{23}^{5-}$, and $H_2P_2Mo_5O_{23}^{4-}$ were derived and used as input for a multivariate curve resolution (MCR) of the CoMoP solution spectra. In this way, a reference spectrum for $H_2PMo_{11}CoO_{40}^{5-}$ in solution was obtained, as well as values for the concentration of all Mo complexes in the CoMoP solutions. The spectrum of the reference solution without any phosphate was used as input for a pure component spectrum of $H_xMo_7O_{24}^{(6-x)-}$ in solution. Pure component spectra for the $H_xP_2Mo_5O_{23}^{(6-x)-}$ complexes were obtained by multivariate curve resolution of a series of spectra taken from 1.0 M Mo/1.0 M phosphate solutions with varying pH. The positions of the main Mo–O stretch vibrations in the pure component spectra are listed in Table 1 and are in good agreement with values presented in literature for these complexes.[13,21,28] The resulting concentration plot of a CoMoP solution, as a function of its phosphate concentration, is given in Figure 4. The agreement between the $H_2PMo_{11}CoO_{40}^{5-}$ concentration obtained by analysis of the Raman and the UV-visible-NIR spectra is remarkable. By comparison with Figure 2, it can be concluded that the main trends are also in good agreement with the calculations. The amount of $H_2PMo_{11}CoO_{40}^{5-}$ formed in the reference solutions is lower than expected from the calculations. However, the calculations are based on formation and stability constants derived from dilute solutions. Details of the data analysis methods applied and the pure component spectra used for the multivariate curve fitting procedures are included in the Supporting Information.

Table 1. Positions for the Mo–O stretch vibrations of the different Mo complexes used as principal components in the multivariate curve resolution of the CoMoP reference solutions Raman spectra.

| | Position of the Mo–O stretch vibrations | | | | |
|---|---|---|---|---|---|
| $H_xMo_7O_{24}^{(6-x)-}$ | 944 (s) | 898 (m) | | | |
| $P_2Mo_5O_{23}^{6-}$ | 956 (w) | 926 (s) | 870 (m) | | |
| $HP_2Mo_5O_{23}^{5-}$ | 936 (s) | 882 (m) | | | |
| $H_2P_2Mo_5O_{23}^{4-}$ | 944 (s) | 894 (m) | | | |
| $H_2PMo_{11}CoO_{40}^{5-}$ | 1008 (w) | 971 (s) | 954 (sh) | 886 (m) | 816 (m) |

**Disintegration of $H_2PMo_{11}CoO_{40}^{5-}$ inside $Al_2O_3$ pellets**: In Figure 5, Raman spectra of the cross-section of γ-$Al_2O_3$ pellets are presented, recorded 15, 60, and 180 min after impregnation with a 1 M Mo $H_2PMo_{11}CoO_{40}^{5-}$ solution. The

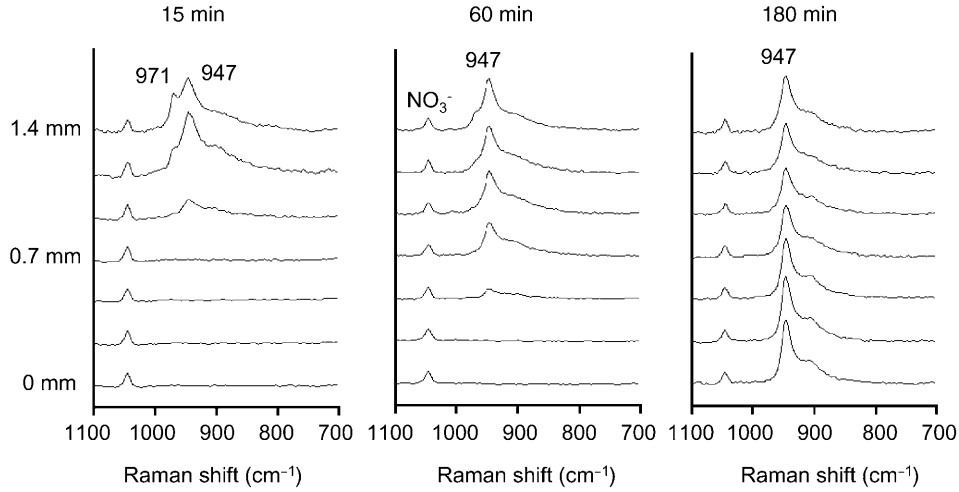


Figure 5. Raman spectra recorded at different positions inside the $Al_2O_3$ support bodies, 15, 60, and 180 min after impregnation with a 1.0 M solution $H_2PMo_{11}CoO_{40}^{5-}$. The distance from the core of the pellets is indicated on the left, whereby 0 mm indicates the center of the pellet and 1.4 mm a position near the exterior surface.

  

measurements were performed at different positions along the axis of the bisected pellets. The presence of $H_2PMo_{11}CoO_{40}^{5-}$ inside the $Al_2O_3$ pores, identifiable by the characteristic Raman peak at 971 $cm^{-1}$, is observed 15 min after impregnation only in the outer shell of the pellets (i.e., 1.4 mm from the core of the pellet). More towards the center of the $Al_2O_3$ bodies, Mo is present as a $H_xMo_7O_{24}^{(6-x)-}$ complex, as can be concluded from the position of the main Mo–O stretch vibration at 947 $cm^{-1}$. Near the core, the absence of any Mo–O vibration peaks indicates that no $Mo^{6+}$-complexes are present. After 60 min, practically all the Mo is present as $H_xMo_7O_{24}^{(6-x)-}$. However, a clear Mo concentration gradient is still present over the pellets, as there is an increase in the relative intensity of the peaks resulting from the Mo–O stretch vibrations in the spectra recorded towards the outside of the pellets. Eventually, after 180 min, a homogeneous distribution of $H_xMo_7O_{24}^{(6-x)-}$ is observed throughout the support bodies; the relative intensity of the 947 $cm^{-1}$ peak, relative to that of the $NO_3^-$ internal standard, is identical for all positions inside the $Al_2O_3$ bodies.

These observations are in agreement with the UV-visible-NIR measurements recorded at the same points in time and at the same positions inside the pellets, as presented in Figure 6. In the spectra recorded near the edge of the bisected pellet, 15 min after impregnation, a clear shoulder is observed at 17600 $cm^{-1}$ and the onset of the $O \rightarrow Mo^{6+}$ charge-transfer band is shifted into the visible region. This confirms the presence of $H_2PMo_{11}CoO_{40}^{5-}$ in the outer shell of the support bodies at this point in time. Towards the core of the pellets, however, all Co seems to be present as $[Co(H_2O)_6]^{2+}$ and the $O \rightarrow Mo^{6+}$ charge-transfer band is absent, validating the Mo concentration gradient observed in the Raman measurements. Eventually, after 180 min, Mo complexes are present throughout the support bodies, as an $O \rightarrow Mo^{6+}$ charge-transfer band is observed for all positions along the cross-section. A homogeneous distribution of $[Co(H_2O)_6]^{2+}$ is already obtained after 60 min, as the intensity of the $Co^{2+}$ d–d transition, with its maximum at 19300 $cm^{-1}$, is the same for all positions along the cross-section.

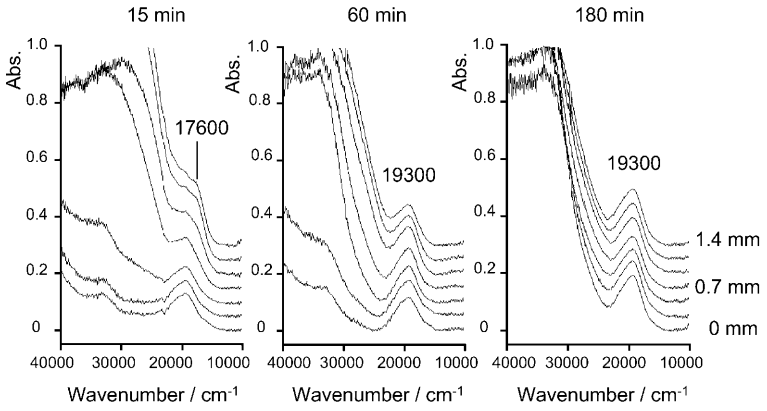


Figure 6. UV-visible-NIR spectra recorded at different positions inside the $Al_2O_3$ support bodies, 15, 60, and 180 min after impregnation with a 1.0 M solution of $H_2PMo_{11}CoO_{40}^{5-}$. The distance from the core of the pellets is indicated on the right.

Upon impregnation of porous support bodies with an aqueous solution, an instantaneous distribution of the liquid phase will occur as a result of the capillary forces that are created by the pore system of the support. However, a strong interaction between the compounds dissolved in the impregnation solution and the support will result in a slower transport of these components.[11–13] After impregnation with a solution containing Co, Mo, phosphate, and nitrate, a different interaction of these components with the $Al_2O_3$ surface is observed. The interaction between the weakly coordinating $NO_3^-$ ion and the support is negligible. This anion is transported with the flow of the solution through the $Al_2O_3$ pores, and within five minutes after impregnation, $NO_3^-$ is detected in the Raman measurements for all positions inside the pellet. For this reason, a homogeneous distribution of this ion can be assumed at all times and this ion can be used as an internal standard in the Raman measurements.[13] After impregnation with the acidic solutions used in this study, the $Al_2O_3$ surface is positively charged, due to the protonation of the basic hydroxyl groups. Hence, Coulomb interaction between the surface and the positively charged Co complexes is limited, and a fast transport of $Co^{2+}$ results in a homogeneous distribution of this complex throughout the support bodies within several minutes. In contrast, electrostatic interaction between the negatively charged Mo complexes and the protonated $Al_2O_3$ hydroxyl groups can be expected. Furthermore, absorption of Mo complexes onto the $Al_2O_3$ surface may take place. Both phenomena result in a much slower distribution of Mo. As was already observed in a previous study,[13] it may take up to 180 min before a homogeneous distribution of Mo is obtained.

Phosphate is known to react with $Al_2O_3$ in acidic environments to form an $AlPO_4$ phase [Eq. (3)].[31,32] In this way, phosphate is withdrawn from the solution inside the $Al_2O_3$ pores. Hence, a decreasing phosphate concentration can be expected towards the center of the pellet. The disintegration of $H_2PMo_{11}CoO_{40}^{5-}$ during impregnation of a 1 M solution of this complex can thus be explained. As the impregnation solution penetrates the pellets, reaction of phosphate with the $Al_2O_3$ results in a lower phosphate concentration in the solution inside the pores of the support. The equilibrium in

Equation (1) shifts to the left and $H_xMo_7O_{24}^{(6-x)-}$ and $[Co(H_2O)_6]^{2+}$ are being formed, which follow their way towards the core of the pellets, each at their own rate.

$$Al_sOH + HPO_4^{2-} + H^+ \rightleftharpoons Al_sHPO_4^- + H_2O \quad (3)$$

The disintegration of $H_2PMo_{11}CoO_{40}^{5-}$ after impregnation onto $Al_2O_3$ is in line with previous studies, in which the instability of these type of complexes on an $Al_2O_3$ support was reported.[22,24] The processes described above are summarized in Figure 7, in which the distribution of the different complexes inside the $Al_2O_3$ pellets at 60 min after impregnation with the $H_2PMo_{11}CoO_{40}^{5-}$ solution is presented in a schematic manner.

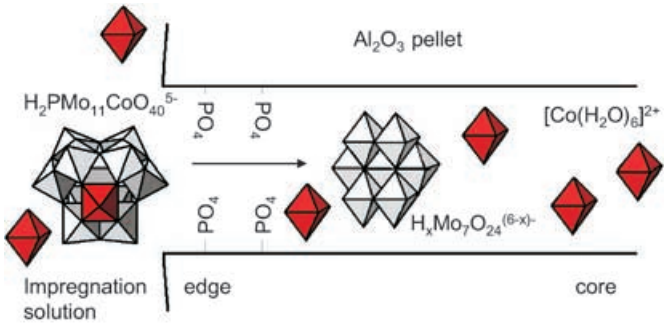


Figure 7. A schematic presentation of the distribution of Mo and Co complexes over an $Al_2O_3$ pellet, 60 min after impregnation with a solution of $H_2PMo_{11}CoO_{40}^{5-}$.

**Formation of $H_2PMo_{11}CoO_{40}^{5-}$ inside $Al_2O_3$ pellets**: From calculations, it can be concluded that in solutions containing Co, Mo, citric acid (CA), and phosphate, with phosphate concentrations of 0.3 M, 0.5 M, and 0.7 M, referred to as CoMoCAP(0.3), CoMoCAP(0.5), and CoMoCAP(0.7), respectively, all citrate (and consequently 40% of all Mo) is bound in a $Mo_4(Hcitrate)_2O_{11}^{4-}$ complex.[25,26] The remaining 0.6 M of $Mo^{6+}$ is contained in $H_xP_2Mo_5O_{23}^{(6-x)-}$. The Raman spectra of the different CoMoCAP($x$) solutions are indeed identical and component analysis shows that they can be reconstructed by the sum of the spectra of $Mo_4(Hcitrate)_2O_{11}^{4-}$ and $H_2P_2Mo_5O_{23}^{4-}$ in solution. At the low pH of these solutions, complexation of $Co^{2+}$ by citrate does not take place and all Co is present in $[Co(H_2O)_6]^{2+}$. Hence, the only difference in the composition of these solutions is the amount of free phosphate present.

In Figure 8, Raman spectra for different positions inside $Al_2O_3$ are presented, 15 min, 240 min, and 24 h after impregnation with the CoMoCAP(0.3) solution. After 15 min, a clear Mo gradient is present over the $Al_2O_3$ pellets, as the intensity of the Mo–O stretch vibration peaks decreases towards the center of the pellet. At this point in time, the presence of a shoulder at 971 $cm^{-1}$ hints at the formation of $H_2PMo_{11}CoO_{40}^{5-}$ in a ring at 0.70–1.17 mm from the center of the extrudates. No Mo complexes are present near the

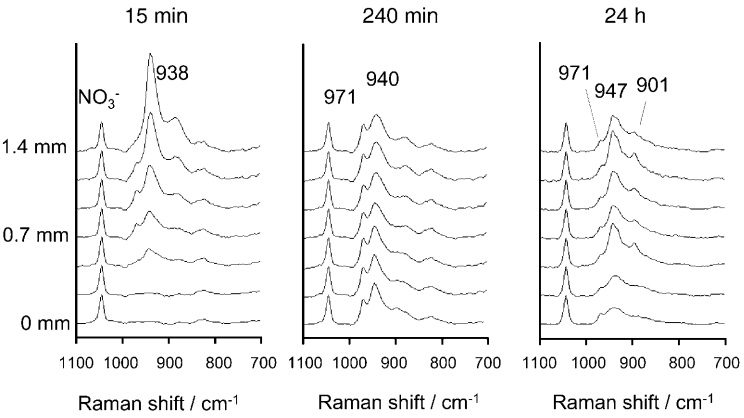


Figure 8. Raman spectra recorded at different positions inside the $Al_2O_3$ support bodies, 15 min, 240 min and 24 h after impregnation with CoMoCAP(0.3) solution. The distance from the core of the pellets is indicated on the left.

core of the pellets at this point in time and it takes several hours before a homogeneous Mo distribution is obtained. After 240 min, $H_2PMo_{11}CoO_{40}^{5-}$ is observed for all positions inside the $Al_2O_3$ pellet. Judging from the constant intensity of the peak at 971 $cm^{-1}$, the distribution of this complex throughout the pellets is rather homogeneous. Besides the heteropolyanion, $H_xP_2Mo_5O_{23}^{(6-x)-}$ seems to be formed at the outside of the pellet, while the much sharper peak at 944 $cm^{-1}$ observed near the core of the pellet is probably due to the formation of $Mo_4(Hcitrate)_2O_{11}^{4-}$. When aging times longer than 8 h are applied, the intensity of the peak at 971 $cm^{-1}$ decreases again and the formation of $Al(OH)_6Mo_6O_{18}^{3-}$ is observed, judging from the emergence of peaks at 947, 901, 570, and 356 $cm^{-1}$.[33] After 24 h, formation of this complex is observed at random positions inside the pellets after 24 h, and the intensity of the characteristic Raman bands differs strongly throughout the sample. This points to the formation of $Al(OH)_6Mo_6O_{18}^{3-}$ crystals inside the $Al_2O_3$ pellets. At positions at which no $Al(OH)_6Mo_6O_{18}^{3-}$ is observed, broad features at 930–950 $cm^{-1}$ indicate the formation of either $H_xP_2Mo_5O_{23}^{(6-x)-}$ or $H_xMo_7O_{24}^{(6-x)-}$. Only small quantities of $H_2PMo_{11}CoO_{40}^{5-}$ remain at this point in time.

The corresponding UV-visible-NIR spectra are presented in Figure 9. After 15 min, the $Co^{2+}$ d–d transition is observed at all positions, while the $O \rightarrow Mo^{6+}$ charge-transfer band is only observed near the edge of the pellets. The presence of $H_2PMo_{11}CoO_{40}^{5-}$ at this point in time is only observed for positions 0.93–1.17 mm from the center of the pellet. The spectra recorded after 240 min are practically identical for all positions. The formation of $H_2PMo_{11}CoO_{40}^{5-}$ is observed throughout the support bodies, indicated by the red-shift of both the onset of the $O \rightarrow Mo^{6+}$ charge-transfer band and the band due to the $Co^{2+}$ d–d transition at 17600 $cm^{-1}$. Eventually the disintegration of the heteropolyanion is again observed and $[Co(H_2O)_6]^{2+}$ is the only Co complex present throughout the pellet after 24 h.

  

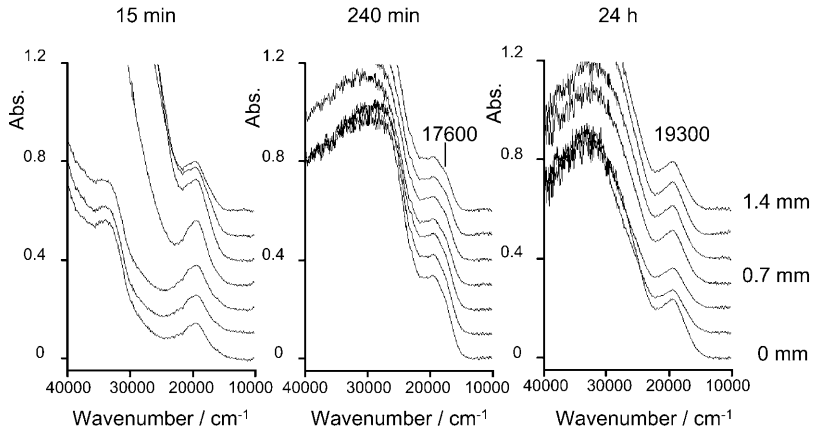


Figure 9. UV-visible-NIR spectra recorded at different positions inside the $Al_2O_3$ support bodies, 15 min, 240 min and 24 h after impregnation with CoMoCAP(0.3) solution. The distance from the core of the pellets is indicated on the right.

The formation of $H_2PMo_{11}CoO_{40}^{5-}$ inside the pellets in the first hours after impregnation with the CoMoCAP(0.3) solution can be explained by using the concepts that were explained in the previous paragraph. The phosphate concentration inside the $Al_2O_3$ pores decreases due to a reaction with the support [Eq. (3)]. Furthermore, the interaction between the phosphate and the support induces an extremely slow transport of phosphate towards the center of the pellets. The occurrence of these concentration gradients results in a different speciation of Mo and Co complexes for different positions inside the support bodies, as changes in the local concentration influence the equilibria in Equations (1) and (2). Apparently, four hours after impregnation, these processes result in a Mo/P ratio that allows for the formation of the heteropolyanion at all positions inside the pellets. Near the outer surface the phosphate concentration is higher than near the core and, as a result, the remaining Mo near the outside of the pellets is contained in $H_xP_2Mo_5O_{23}^{(6-x)-}$, while more towards the interior, $Mo_4(Hcitrate)_2O_{11}^{4-}$ is formed.

The formation of $Al(OH)_6Mo_6O_{18}^{3-}$ is reported for the impregnation of $Al_2O_3$ with $(NH_4)_6Mo_7O_{24}{\cdot}4H_2O$ (AHM) solutions, when long aging times are applied.[34,35] This Anderson-type heteropolyanion is formed by ligand-promoted dissolution of $Al^{3+}$ ions in a reaction represented in Equation (4).

$$6\,H_xMo_7O_{24}^{6-} + 7\,Al^{3+} + 24\,H_2O \rightleftharpoons 7\,Al(OH)_6Mo_6O_{18}^{3-} \quad (4)$$

Due to its low solubility, precipitation of this complex takes place. The $Al^{3+}$ ions are constantly generated by dissolution of the $Al_2O_3$ support, as impregnation was carried out with an acidic solution. This results in a chain reaction in which, in time, increasing amounts of $Al(OH)_6Mo_6O_{18}^{3-}$, and eventually crystals are formed.[35] This unwanted process may be prevented by the addition of complexing agents to the impregnation solution.[13] In this case, the formation of this complex at 24 h after impregnation becomes possible, as the concentration of complexing agents, after reaction of the phosphate with the $Al_2O_3$, is insufficient to accommodate all Mo present. The $Al(OH)_6Mo_6O_{18}^{3-}$ starts to form and the concentration of Mo in the solution inside the pores decreases, due to the precipitation of this complex. The resulting increase in the P/Mo ratio causes the formation of $H_xP_2Mo_5O_{23}^{(6-x)-}$ at the expense of $H_2PMo_{11}CoO_{40}^{5-}$, according to Equation (2).

When impregnation was carried out with a 1.0 M Mo, 0.5 M Co, 0.3 M P solution without citrate, the formation of $H_2PMo_{11}CoO_{40}^{5-}$ was not observed. This beneficial effect of citrate is not yet fully understood. It is known that citrate forms extremely stable complexes with Mo at low pH.[13] In this way, the presence of citrate prevents the absorption of Mo onto the $Al_2O_3$ surface after impregnation. Consequently, a high concentration of Mo inside the pores is maintained, enough Mo is present for the formation of the heteropolyanion, and the P/Mo ratio is kept sufficiently low. Furthermore, the presence of citrate prevents the formation of $Al(OH)_6Mo_6O_{18}^{3-}$ and the resulting disintegration of $H_2PMo_{11}CoO_{40}^{5-}$ as described in the previous paragraph.[13] Finally, impregnation of $Al_2O_3$ pellets with an acidic solution will result in an increase in the pH of the solution, due to the buffering effect of the support. The addition of citrate could counteract this effect, making sure that the pH of the solution inside the $Al_2O_3$ pores remains sufficiently low for the formation of $H_2PMo_{11}CoO_{40}^{5-}$. However, the validity of these assumptions is difficult to prove with the current techniques. In Figure 10, a simplified representation is given for the speciation of the different complexes, 60 minutes after

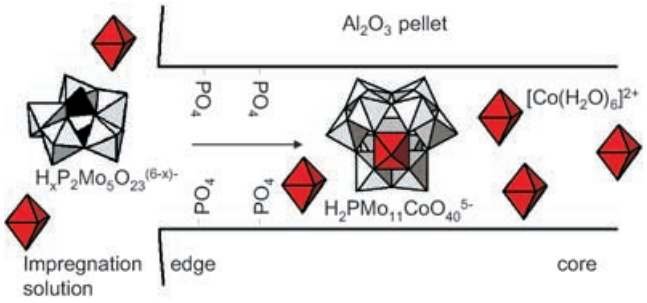


Figure 10. A schematic presentation of the distribution of Mo and Co complexes over an $Al_2O_3$ pellet, 60 min after impregnation with a CoMoCAP(0.3) solution.

impregnation with the CoMoCAP(0.3) solution used in this study.

**Monitoring the distribution of $H_2PMo_{11}CoO_{40}^{5-}$ inside $Al_2O_3$ pellets**: By using the $NO_3^-$ peak as an internal standard, the local concentration of $H_2PMo_{11}CoO_{40}^{5-}$ inside of the $Al_2O_3$ pores was determined for the different positions inside the pellets. In principle, this could be done in much the same way as was done for the CoMoP solutions. However, the presence of adsorbed Mo complexes, $H_xMo_7O_{24}^{(6-x)-}$, $Mo_4(Hcitrate)_2O_{11}^{4-}$, and $H_xP_2Mo_5O_{23}^{(6-x)-}$ in different protonation states all give rise to Mo–O stretch vibrations at a slightly different frequency between 930 and 945 $cm^{-1}$. Furthermore, the quality of the data obtained by measurements on the impregnated $Al_2O_3$ pellets is of inferior quality relative to measurements on solutions. Therefore, a different approach was taken to obtain semiquantitative distribution profiles of the heteropolyanion across the pellets. The pure component spectrum of $H_2PMo_{11}CoO_{40}^{5-}$ in solution, as derived from analysis of the CoMoP reference solutions, was used in a fit of the spectra recorded on the bisected pellets. Further information on the quantitative analysis of the Raman spectra can be found in the Supporting Information. Distribution profiles of $H_2PMo_{11}CoO_{40}^{5-}$ inside the $Al_2O_3$ pellets, at 4 and 24 h after impregnation with solutions of CoMoCAP(0.3), CoMoCAP(0.5), and CoMoCAP(0.7) are presented in Figure 11. From these profiles it is evident that the formation of $H_2PMo_{11}CoO_{40}^{5-}$ is observed at different positions in the pellets when the different CoMoCAP solutions were used for impregnation. For instance, 4 h after impregnation with a CoMoCAP(0.3) solution, a reasonably homogeneous distribution of the desired complex is achieved, as was discussed in the previous section. For all positions, the concentration of Mo contained in the heteropolyanion is approximately 0.55 M. In contrast, at the same point in time after impregnation with a CoMoCAP(0.7) solution, $H_2PMo_{11}CoO_{40}^{5-}$ formation only takes place near the core of the pellets. In the remaining part of the sample, Mo is present as $H_xP_2Mo_5O_{23}^{(6-x)-}$. This is due to the phosphate concentration gradient, which is still present at this point in time. The P/Mo ratio near the core of the pellets is sufficiently low to allow for the formation of $H_2PMo_{11}CoO_{40}^{5-}$, while the high P/Mo ratio near the exterior of the bodies results in the formation of $H_xP_2Mo_5O_{23}^{(6-x)-}$. A slight concentration gradient is observed after impregnation with the CoMoCAP(0.5) solution and this can be regarded as an intermediate case.

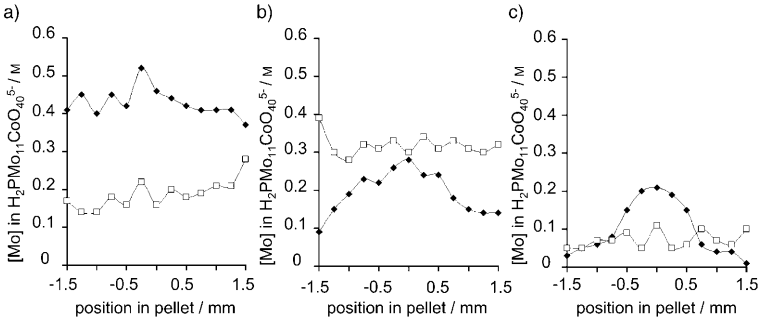


Figure 11. Distribution profiles of $H_2PMo_{11}CoO_{40}^{5-}$ inside the pores of the $Al_2O_3$ pellets 4 h (◆) and 24 h (□) after impregnation with a) CoMoCAP(0.3), b) CoMoCAP(0.5), and c) CoMoCAP(0.7) solutions.

After 24 h, no gradient is observed in the $H_2PMo_{11}CoO_{40}^{5-}$ distribution for any of the samples. A considerable amount of $H_2PMo_{11}CoO_{40}^{5-}$ is present in the CoMoCAP(0.5) sample. In the pellets impregnated with the CoMoCAP(0.3) solution, the formation of $Al(OH)_6Mo_6O_{18}^{3-}$ takes place, as was discussed above. $H_xP_2Mo_5O_{23}^{(6-x)-}$ is predominantly present in the sample impregnated with the CoMoCAP(0.7) solution, as the P/Mo ratio is too high for all positions when a homogeneous distribution of phosphate is obtained. In brief, the observed $H_2PMo_{11}CoO_{40}^{5-}$ distribution profiles can be explained by the occurrence of phosphate concentration gradients after impregnation with an acidic CoMoCAP solution. By controlling these phosphate gradients, the distribution of the heteropolyanion can be tuned. It is anticipated that a similar approach can be used for the deposition of a whole range of phosphate-containing Keggin ions onto $Al_2O_3$ bodies.

**Spatially resolved spectroscopic techniques in the preparation of supported catalyst bodies**: This study is, to the best of our knowledge, the first example of how the application of complementary, spatially resolved, spectroscopic techniques can be of great value in designing supported catalyst bodies. For the identification of $H_2PMo_{11}CoO_{40}^{5-}$, a combination of Raman and UV-visible-NIR spectroscopy is essential, as in this way the coordination of both Co and Mo can be revealed. Undoubtedly, in companies dealing with catalyst preparation, a lot of know-how is present on this subject. However, in studies that are reported in the literature into the preparation of supported catalyst bodies, not much attention has been paid to the effect of concentration profiles that occur after the impregnation of support bodies. Generally, if one strives to prepare a catalyst with a certain transition-metal complex present on the support, impregnation is simply carried out with a solution containing this specific complex. Why this approach is not always successful was illustrated by the disintegration of the $H_2PMo_{11}CoO_{40}^{5-}$ complex after impregnation with a solution of $H_2PMo_{11}CoO_{40}^{5-}$.

In this study, it was also shown that one can take advantage of the concentration profiles that are established over support bodies after impregnation to form the desired complex inside the pores of the support at specific positions inside catalyst bodies. In this way, systems with different cat-

  

alytic functions within a single catalyst body could be created with relatively simple means. In the field of hydrotreating catalysis in particular, extrudates with spatially controlled hydrodesulfurization and hydrodemetallization functions could be envisaged. This study can therefore be seen as a step towards a more rational approach in the preparation of supported catalyst bodies. In this respect, the application of spectroscopic techniques, which allow one to monitor these systems throughout their preparation is highly valuable. With the information obtained in this way, the preparation procedure, in which the composition of the impregnation solution and aging time are important factors, can be optimized in a much more rational way. It is clear that drying and calcination of these systems may have a severe influence on the nature and distribution of the metal complexes inside the $Al_2O_3$ pellets, as well. Both techniques used in this study can also be applied on dried and calcined samples. Indeed, studies are ongoing in our group to probe the physicochemical processes during drying and calcination of CoMoP/$Al_2O_3$ systems by using a similar approach.[36] As a large variety of metal complexes show d–d or charge-transfer transitions, the presented UV-visible-NIR microspectroscopy method is generally applicable to study their speciation inside the pores of oxidic support bodies. Spatially resolved Raman spectroscopy can be applied to study the preparation of metal oxide catalyst bodies, since the $MO_x$ vibrations in these compounds generally give rise to strong signals in Raman spectroscopy.

## Conclusion

The power of combining Raman microscopy and UV-visible-NIR microspectroscopy to obtain insight into the physicochemical processes that occur during the preparation of supported catalysts was illustrated by monitoring the disintegration and formation of $H_2PMo_{11}CoO_{40}^{5-}$ inside $Al_2O_3$ bodies. The distribution of Mo and Co complexes inside the pores of $Al_2O_3$ pellets was studied after impregnation with solutions of CoMoP of different constitution, by using the aforementioned techniques. First, from combined Raman and UV-visible-NIR measurements on solutions of CoMoP, the optimal conditions for $H_2PMo_{11}CoO_{40}^{5-}$ formation (P/Mo ratio 0.15, pH 4) were determined. At the same time, the Raman spectrum for the heteropolyanion in solution was derived by multivariate curve resolution (MCR), which was used in a later stage to determine the concentration of this complex inside the pores of $Al_2O_3$. It was shown that after impregnation with a solution of $H_2PMo_{11}CoO_{40}^{5-}$, disintegration of this complex takes place due to a reaction of phosphate with the $Al_2O_3$ surface. As a result of this reaction, $H_xMo_7O_{24}^{(6-x)-}$ and $[Co(H_2O)_6]^{2+}$ are formed. As the interaction of Co complexes with the $Al_2O_3$ surface is weak, transport of $[Co(H_2O)_6]^{2+}$ is fast, and a homogeneous distribution of this complex is achieved almost instantaneously. Transport of negatively charged Mo complexes is slow after impregnation with an acidic solution, and aging times of several hours are required to obtain full equilibration of the system.

In an alternative approach, the formation of $H_2PMo_{11}CoO_{40}^{5-}$ inside the $Al_2O_3$ pellets was achieved by the addition of citrate and extra phosphate to the impregnation solution. The reaction of free phosphate with the support results in a lower phosphate concentration inside the pores, creating the right conditions for $H_2PMo_{11}CoO_{40}^{5-}$ to be formed. The strong interaction between phosphate and $Al_2O_3$ leads to strong concentration gradients of this component over the support bodies in the first hours after impregnation. These gradients may be used to prepare catalyst bodies with different $H_2PMo_{11}CoO_{40}^{5-}$ distributions. In our view, this study clearly illustrates how the possibility of monitoring the distribution of metal complexes in support bodies throughout the preparation process can greatly enable the preparation of industrial supported catalysts in a controlled manner.

## Experimental Section

Pore volume impregnation was carried out on cylindrical $\gamma$-$Al_2O_3$ pellets (Engelhard). These were calcined at 600 °C for 6 h and stored at 120 °C before impregnation. The pore volume of this support material was 1.1 mL g$^{-1}$, and its surface area 200 m$^2$g$^{-1}$. The pellets were 3 mm in both length and diameter. All impregnation solutions contained 1.0 M Mo and 0.5 M Co, yielding a 15 wt% $MoO_3$ and a 7.6 wt% CoO loading in the final catalyst. During impregnation, care was taken that the solution was distributed homogeneously over all $Al_2O_3$ bodies and the pellets were kept in a closed vessel after impregnation. At several points in time a pellet was collected from the impregnation vessel and a cross-section was made perpendicular to the axis of the cylinder, using a razorblade.

Raman spectra were recorded on these bisected pellets by using a Kaiser RXN spectrometer equipped with a 785 nm diode laser in combination with a Hololab 5000 Raman microscope. A 10× lens was used for beam focusing and collection of scattered radiation, resulting in a spot size on the sample of approximately 50 μm. The laser power on the sample was 100 mW. For a typical measurement, 5 spectra were accumulated with a 3 s exposure time. Background correction was carried out by subtraction of a reference spectrum recorded on wet $Al_2O_3$ and the spectra were scaled to the $NO_3^-$ peak at 1048 cm$^{-1}$, which can be used as an internal standard. UV-visible-NIR spectra were recorded in much the same way using a specially designed set-up for spatially resolved UV-visible-NIR measurements. In this set-up, a measurement spot on the sample of approximately 100 μm is created by using optical fibers. Scans were made across the cross-section of bisected pellets with the use of a remote-controlled *x*-*y*-*z* stage. During UV-visible-NIR measurements, the sample was placed in a humidity controlled measuring cell to prevent dehydration. Specifications of this apparatus have been reported elsewhere.[14]

The speciation of Co and Mo complexes in CoMoP solutions was studied. A solution was prepared from $MoO_3$ (Acros, p.a.) and $Co(NO_3)_2{\cdot}6H_2O$ (Acros, p.a.), containing 1.0 M Mo, and 0.5 M Co, which was titrated with a solution containing 1.0 M Mo, 0.5 M Co and 1.0 M phosphate (85% $H_3PO_4$ (Merck, p.a.)). In this way, a series of reference solutions with a phosphate concentration between 0 and 0.5 M was prepared. The composition of these solutions was calculated with the help of a computer program, which contains equilibrium and formation constants for the different complexes.[25,26] UV-visible-NIR spectra of these solutions were recorded by using a Varian Cary 50 UV-visible spectrophotometer equipped with optical fibers and a Hellma immersion probe for measurements in solution. The path length of the light through the solution was 2 mm. Raman spectra were recorded simultaneously by using a Kaiser RXN spectrometer equipped with a 532 nm diode laser. Raman measurements were also

carried out, in the same way, on a series of 1.0 M Mo, 1.0 M phosphate solutions, in the pH range of 1.40–8.90, to obtain reference spectra of $H_xP_2Mo_5O_{23}^{(6-x)-}$ in its different protonation states. Details on the procedures followed for the analysis of the Raman spectra can be found in the Supporting Information.

For impregnation, a solution which predominantly contains $H_2PMo_{11}CoO_{40}^{5-}$ was prepared. To this end, the appropriate amount of $CoCO_3$ (Acros, p.a.) was added to a boiling suspension of $MoO_3$ in 0.3 M $HNO_3$. After stirring for 120 min, the resulting red solution was allowed to cool down to room temperature and 85 wt% $H_3PO_4$ solution was added to obtain a phosphate concentration of 0.1 M. Solutions containing 1.0 M Mo, 0.5 M Co, and 0.2 M citric acid with different $PO_4^{3-}$ concentrations were prepared by dissolving appropriate amounts of $(NH_4)_6Mo_7O_{24}\cdot 4H_2O$ (Acros, p.a.), $Co(NO_3)_2\cdot 6H_2O$, crystalline citric acid (OPG Pharma, p.a.), and an 85 wt% $H_3PO_4$ aqueous solution. Solutions were prepared with phosphate concentrations of 0.3 M, 0.5 M, and 0.7 M, referred to as CoMoCAP(0.3), CoMoCAP(0.5), and CoMoCAP(0.7), respectively. Impregnation was carried out with these solutions as well. The chemical composition and final pH of the different solutions used for impregnation are presented in Table 2.

Table 2. Chemical composition (concentration) and pH of the impregnation solutions used in this study.

| | Mo [M] | Co [M] | P [M] | Citrate [M] | pH |
|---|---|---|---|---|---|
| $H_2PMo_{11}CoO_{40}^{5-}$ | 1.00 | 0.50 | 0.10 | – | 2.4 |
| CoMoCAP(0.3) | 1.00 | 0.50 | 0.30 | 0.20 | 1.2 |
| CoMoCAP(0.5) | 1.00 | 0.50 | 0.50 | 0.20 | 1.1 |
| CoMoCAP(0.7) | 1.00 | 0.50 | 0.70 | 0.20 | 1.0 |

## Acknowledgements

The authors acknowledge valuable discussions with Marcel Jansen, Jan Nieman, Eelco Vogt (Albemarle Catalysts BV), and Brenda Rossenaar (Akzo Nobel Chemicals Research). B.M.W. acknowledges financial support by the Dutch National Science Foundation (NWO-CW-van der Leeuw and VICI grants) and NRSC-Catalysis. Part of this research has been sponsored by Albemarle Catalysts BV.

[1] J. Hagen, *Industrial Catalysis: A Practical Approach*, Wiley-VCH, Weinheim, **1999**.
[2] G. Ertl, H. Knozinger, J. Weitkamp, *Preparation of Solid Catalysts*, Wiley-VCH, Weinheim, **1999**.
[3] I. E. Wachs, B. M. Weckhuysen in *Handbook of Surfaces and Interfaces of Materials; Surface and Interface Phenomena* (Ed.: H. S. Nalwa), Academic Press, San Diego, **2001**, pp. 613–648.
[4] A. T. Bell, *Science* **2003**, *299*, 1688–1691.
[5] R. Schlogl, S. B. Abd Hamid, *Angew. Chem.* **2004**, *116*, 1656–1667; *Angew. Chem. Int. Ed.* **2004**, *43*, 1628–1637.
[6] K. P. de Jong, *CATTECH* **1998**, *2*, 87–95.
[7] K. P. de Jong, *Curr. Opin. Solid State Mater. Sci.* **1999**, *4*, 55–62.
[8] A. Lekhal, B. J. Glasser, J. G. Khinast, *Chem. Eng. Sci.* **2004**, *59*, 1063–1077.
[9] M. Komiyama, *Catal. Rev. Sci. Eng.* **1985**, *27*, 341–372.
[10] A. Lekhal, B. J. Glasser, J. G. Khinast, *Chem. Eng. Sci.* **2001**, *56*, 4473–4487.
[11] S. Y. Lee, R. Aris, *Catal. Rev.-Sci. Eng.* **1985**, *27*, 207–340.
[12] A. V. Neimark, L. I. Kheifez, V. B. Fenelonov, *Ind. Eng. Chem. Prod. Res. Dev.* **1981**, *20*, 439–450.
[13] J. A. Bergwerff, T. Visser, R. G. Leliveld, B. A. Rossenaar, K. P. de Jong, B. M. Weckhuysen, *J. Am. Chem. Soc.* **2004**, *126*, 14548–14556.
[14] L. G. A. van de Water, J. A. Bergwerff, T. A. Nijhuis, K. P. de Jong, B. M. Weckhuysen, *J. Am. Chem. Soc.*, **2005**, *127*, 5024–5025.
[15] J. V. Lauritsen, S. Helveg, E. Laegsgaard, I. Stensgaard, B. S. Clausen, H. Topsoe, E. Besenbacher, *J. Catal.* **2001**, *197*, 1–5.
[16] R. Prins, V. H. J. Debeer, G. A. Somorjai, *Catal. Rev.-Sci. Eng.* **1989**, *31*, 1–41.
[17] J. Grimblot, *Catal. Today* **1998**, *41*, 111–128.
[18] R. Cattaneo, F. Rota, R. Prins, *J. Catal.* **2001**, *199*, 318–327.
[19] L. Medici, R. Prins, *J. Catal.* **1996**, *163*, 38–49.
[20] L. Coulier, V. H. J. de Beer, J. A. R. van Veen, J. W. Niemantsverdriet, *J. Catal.* **2001**, *197*, 26–33.
[21] A. Griboval, P. Blanchard, E. Payen, M. Fournier, J. L. Dubois, *Catal. Today* **1998**, *45*, 277–283.
[22] A. Griboval, P. Blanchard, L. Gengembre, E. Payen, M. Fournier, J. L. Dubois, J. R. Bernard, *J. Catal.* **1999**, *188*, 102–110.
[23] C. I. Cabello, I. L. Botto, H. J. Thomas, *Appl. Catal. A* **2000**, *197*, 79–86.
[24] K. Y. Lee, M. Misono in *Preparation of Solid Catalysts* (Eds.: G. Ertl, H. Knozinger, J. Weitkamp), Wiley-VCH, Weinheim, **1999**, pp. 240–261.
[25] L. Pettersson, I. Andersson, L.-O. Öhman, *Inorg. Chem.* **1986**, *25*, 4726–4733.
[26] J. J. Cruywagen, E. A. Rohwer, G. F. S. Wessels, *Polyhedron* **1995**, *14*, 3481–3493.
[27] M. Leyrie, M. Fournier, R. Massart, *C. R. Acad. Sci. Paris* **1971**, *273*, 1569–1572.
[28] G. Mestl, T. K. K. Srinivasan, *Catal. Rev.-Sci. Eng.* **1998**, *40*, 451–570.
[29] A. B. P. Lever, *Inorganic Electronic Spectroscopy*, Elsivier, Amsterdam, **1984**.
[30] R. S. Weber, *J. Catal.* **1995**, *151*, 470–474.
[31] J. A. R. Van Veen, P. Hendriks, E. Romers, R. R. Andrea, *J. Phys. Chem.* **1990**, *94*, 5275–5282.
[32] J. A. R. Van Veen, P. Hendriks, R. R. Andrea, E. Romers, A. E. Wilson, *J. Phys. Chem.* **1990**, *94*, 5282–5285.
[33] L. Le Bihan, P. Blanchard, M. Fournier, J. Grimblot, E. Payen, *J. Chem. Soc. Faraday Trans.* **1998**, *94*, 937–940.
[34] X. Carrier, J. F. Lambert, S. Kuba, H. Knozinger, M. Che, *J. Mol. Struct.* **2003**, *656*, 231–238.
[35] X. Carrier, J. F. Lambert, M. Che, *J. Am. Chem. Soc.* **1997**, *119*, 10137–10146.
[36] L. G. A. van de Water, J. A. Bergwerff, R. G. Leliveld, B. M. Weckhuysen, K. P. de Jong, unpublished results *J. Phys. Chem. B.*, in press.

Received: February 1, 2005
Published online: May 13, 2005

  